Journal of Volcanology and Geothermal Research 397 (2020) 106832

Contents lists available at ScienceDirect

Journal of Volcanology and Geothermal Research

journal homepage: www.elsevier.com/locate/jvolgeores

Implications of deflation-inflation event models on Kīlauea Volcano, Hawai'i

Alyssa N. Anderson [a,b,*], James H. Foster [a], Neil Frazer [b]

[a] Hawai'i Institute of Geophysics and Planetology, University of Hawai'i at Mānoa, Honolulu, HI, USA
[b] Department of Earth Sciences, University of Hawai'i at Mānoa, Honolulu, HI, USA

ARTICLE INFO

Article history:
Received 25 July 2019
Received in revised form 26 February 2020
Accepted 27 February 2020
Available online 5 March 2020

Keywords:
Kīlauea
magma reservoir
deflation-inflation event
modeling

ABSTRACT

Surface deformation of volcanic areas can reveal information about subsurface magma reservoirs and how magma is transported between them, which is an important part of volcano monitoring for hazard mitigation. One prominent style of deformation observed at Kīlauea volcano, Hawai'i, is episodic deflation-inflation (DI) events, which are recorded in surface deformation data and characterized by deflation of the summit region over hours to days followed by rapid re-inflation. The exact cause of DI events is unknown, however, a commonly proposed explanation is that a temporary blockage occurs in the conduit connecting the south caldera magma reservoir to the shallower Halema'uma'u reservoir, thus interrupting the influx of magma. This model is investigated by testing the hypothesis that during the deflationary phase of a DI event, the volume of magma blocked from reaching the Halema'uma'u reservoir is added to the south caldera reservoir. Using a mass balance approach and deformation modeling, the expected deformation (tilt) pattern was predicted for the reservoirs and compared to tilt observations from 16 large (>4 μrad magnitude) DI events between 2010 and 2012. While the predicted tilts due to inflation from the south caldera reservoir are strong enough to be detected, this signal is not seen in the tilt observations. We also explore the possibility that the blockage occurs below the south caldera reservoir, as well as alternative configurations that include a direct connection between the south caldera reservoir and the eruption site. None of the simple two-reservoir models we test are able to adequately satisfy the observations. Selected DI events show that tilt vectors change in both magnitude and azimuthal direction over the course of deflation. We conclude that the portion of the summit storage and plumbing system active during these DI events is more complicated than two connected chambers, and that it is more likely that these summit reservoirs have their own source conduits connecting in some complex way to the deep magma source.

1. Introduction

Episodic deformation caused by pressure perturbations within a volcano's magmatic system can reveal important information about magma storage and transport necessary to volcano monitoring for hazard mitigation (e.g., Voight et al., 1998; Yamashina et al., 1999 Cervelli and Miklius, 2003; Anderson et al., 2010, 2015; Genco and Ripepe, 2010; Poland et al., 2014). At Kīlauea volcano, Hawai'i, episodic deformation has been related to eruptive activity (Swanson et al., 1979; Wolfe et al., 1987), and investigated through modeling of geodetic deformation sources in order to make interpretations about the shallow magmatic system configuration (Dvorak and Okamura, 1987; Dvorak and Dzurisin, 1997). In the 1990s a new type of episodic deformation, deflation-inflation (DI) events, was observed (Heliker and Mattox, 2003) and has since been a frequent signal associated with the summit region, recorded especially well by the summit tiltmeter network. A common explanation for these events is that a blockage occurs within the magmatic plumbing system, temporarily cutting off the supply of magma into the shallow summit reservoir while magma continues to exit through a conduit to the eruption site (Cervelli and Miklius, 2003; Anderson et al., 2015). DI events are most commonly associated with activity in the shallow Halema'uma'u reservoir (HMMR), but their relationship with the deeper south caldera reservoir (SCR) is not often discussed in detail. The SCR is thought to be directly connected to the HMMR, which implies that the SCR should also be affected by these events. In a comprehensive study on DI events, Anderson et al. (2015) note that while DI events have not previously been known to manifest in the SCR, potential deformation related to the SCR during the events could go undetected, and that certain types of events could be caused by blockages deeper within the magmatic system.

The work presented here investigates the role of the SCR during DI events, which provides insight to the cause of DI events and therefore the magmatic plumbing system dynamics of Kīlauea. We explore the implications of the model for DI events proposed by Cervelli and

* Corresponding author at: University of Hawai'i at Mānoa, 1680 East-West Road, Honolulu, HI 96822, USA.
E-mail address: ananders@hawaii.edu (A.N. Anderson).

https://doi.org/10.1016/j.jvolgeores.2020.106832
0377-0273/

Miklius (2003). Under these assumptions, we use a geodetic model to determine the expected extent of SCR related tilt deformation during DI events, and test if that deformation is detectable over the contribution from the HMMR. We compare model predictions with tilt observations for 16 large (>4 μrad magnitude) DI events that occurred between January 9, 2010 and January 5, 2012.

2. Background

2.1. Existing model of Kīlauea summit

Kīlauea volcano (Fig. 1) is located on the island of Hawai'i on the south flank of Mauna Loa volcano, and is characterized by a main summit caldera, the Southwest Rift Zone (SWRZ), and East Rift Zone (ERZ) (Holcomb, 1987; Fiske et al., 1993). Magma is supplied from depth and rises to the summit where it is stored and transported (Eaton and Murata, 1960; Tilling and Dvorak, 1993). Previous studies have used a variety of datasets to model the location, size, and depth of the main summit magma reservoirs (Cervelli and Miklius, 2003; Baker and Amelung, 2012; Poland et al., 2012). The SCR is generally considered to be the main storage area and location of long-term deformation, sitting at a depth of ~3 km below the southern caldera region (Delaney et al., 1990, 1993; Cervelli and Miklius, 2003; Baker and Amelung, 2012; Poland et al., 2012; Poland et al., 2014). The Halema'uma'u magma reservoir (HMMR) is a shallower and smaller storage area located in the region east to southeast of Halema'uma'u crater at 1–2 km depth, as suggested by studies of deformation (Fiske and Kinoshita, 1969; Dvorak and Okamura, 1987; Johnson, 1992; Cervelli and Miklius, 2003; Poland et al., 2014), gravity, (Dzurisin et al., 1980; Johnson et al., 2010) and seismicity (Ohminato et al., 1998; Almendros et al., 2002; Chouet et al., 2010; Dawson et al., 1999; Battaglia et al., 2003; Okubo et al., 2014). Because extensive work has already been done to model these reservoirs, we use previously estimated reservoir parameters for our models.

A third recognized storage area is beneath the Keanakāko'i crater zone. This region has been found to be periodically active in the last few decades (Dvorak and Okamura, 1987; Klein et al., 1987; Yang et al., 1992; Poland et al., 2014), but its connection to the other zones is unclear. Storage areas have also been proposed in the SWRZ with a connection to the summit (Holcomb, 1987; Fiske et al., 1993; Myer et al., 2008; Baker and Amelung, 2012; Poland et al., 2012). A magmatic connection exists from the summit to the ERZ based on the correlation of summit draining to eruptive activity along the ERZ, where Kīlauea had been erupting almost continuously since 1983 mainly from the Pu'u 'Ō'ō vent until May 2018 (Swanson et al., 1979; Wolfe et al., 1987; Owen et al., 2000; Heliker and Mattox, 2003; Poland et al., 2009b; Montgomery-Brown et al., 2010; Baker and Amelung, 2012; Lundgren et al., 2013). The exact nature and location of the connection between the summit and the ERZ is uncertain. The correlation of pressure perturbations at the HMMR and slightly later at Pu'u 'Ō'ō (Cervelli and Miklius, 2003) indicates a relatively direct connection between the HMMR and ERZ, while seismic observations indicate a deeper connection (Klein et al., 1987).

2.2. Deflation-inflation events

DI events are characterized by radial deflation of the summit area lasting hours to days, followed by a nearly instantaneous transition to rapid inflation, with deformation appearing radially outwards from a point within the caldera region east and southeast of Halema'uma'u crater. While the exact processes responsible for DI events are unclear, it is assumed that the signals are caused by outflux from the summit temporarily exceeding magma input (Anderson et al., 2015). Pressure perturbations have been attributed to a temporary blockage that interrupts the influx of magma within the shallow magmatic system (Cervelli and Miklius, 2003; Anderson et al., 2015). Poland et al. (2009a) proposed a convective overturn model for the cause of the events, which involves gas-rich magma replacing degassed magma. DI events can propagate down the ERZ after occurring at the summit, and have been recorded as matching, time-delayed signals at a tiltmeter located at Pu'u 'Ō'ō, implying a connection between the summit and ERZ vent (Cervelli and Miklius, 2003).

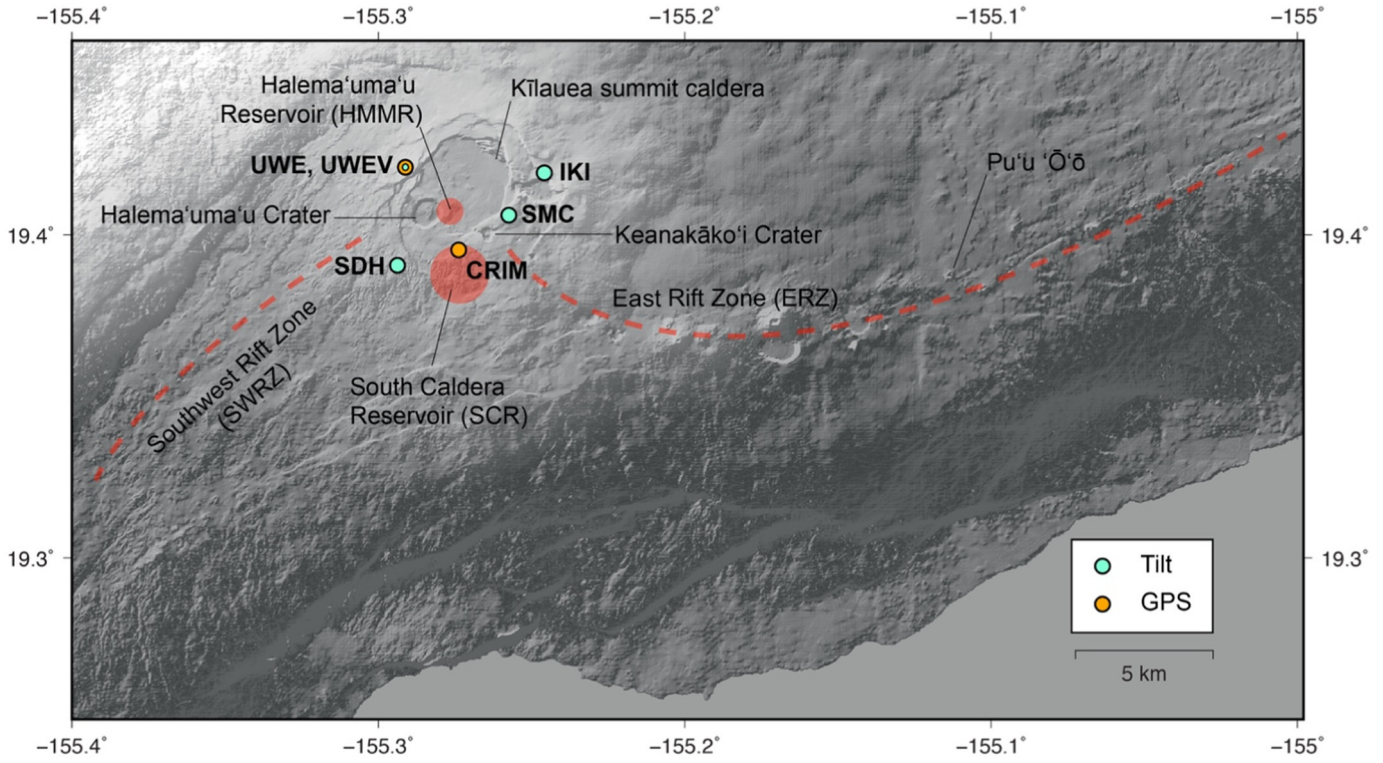

Fig. 1. Kīlauea volcano with locations of instruments and geologic features discussed in this study. Size and location of reservoirs are approximate.

DI pressure changes measured by tiltmeters were also found to be correlated with the height of the level of the summit lava lake open between 2008 and 2018 within Halemaʻumaʻu crater (Orr et al., 2013; Patrick et al., 2013; Patrick and Orr, 2013). Lava lake surface heights at Kīlauea have been related to deformation and used as a pressure gauge for the associated magma reservoir (Tilling, 1987; Johnson, 1992; Denlinger, 1997; Segall et al., 2001). Anderson et al. (2015) used the tilt and lava lake level relationship to estimate the relationship between volume and pressure changes, and refine the geometry of the summit magma reservoir. Seismic tremor has also been associated with DI events (Cervelli and Miklius, 2003; Dawson et al., 2004) and other tilt signals (Ohminato et al., 1998).

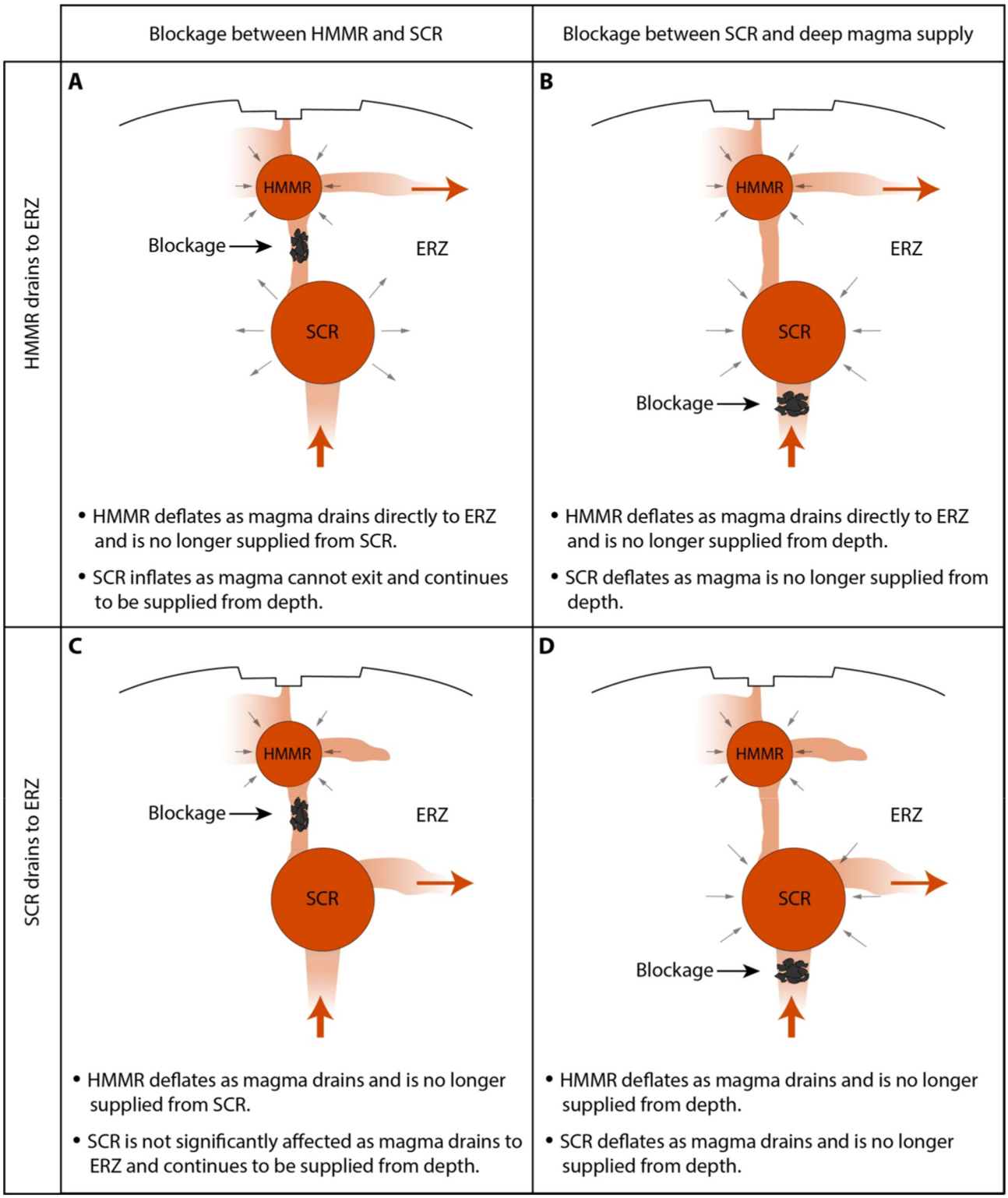

Fig. 2. Schematic cross sections of Kīlauea's magmatic plumbing system showing locations of magma pathways and blockages and their implications on reservoir volumes during DI events. Relative sizes and distances are not to scale. HMMR = Halemaʻumaʻu reservoir, SCR = south caldera reservoir, ERZ = east rift zone.

3. Motivation: implications of DI model scenarios

During DI events, the location of the temporary blockage and the configuration of magma pathways will influence the resulting pressure changes in the magma reservoirs. Fig. 2 illustrates four such scenarios and their implications for the system. In all the configurations, magma is supplied from depth to the SCR where it is then transported through a conduit to the HMMR. Magma can drain to the ERZ from either the HMMR (Fig. 2A and B) or from the SCR (Fig. 2C and D). For each of these cases, the blockage can occur between the conduit connecting the SCR and the HMMR (Fig. 2A and C), or between the SCR and its magma supply from depth (Fig. 2B and D).

The summit configuration proposed by Poland et al. (2014) does not include a conduit directly connecting the HMMR to the ERZ, and instead, based on seismic data, favors a connection from the SCR to the ERZ (Fig. 2C and D). In this scenario, if the blockage occurs in the conduit between the reservoirs, then magma in the HMMR must be able to rapidly drain somewhere other than the ERZ when its supply is cut off, in order to produce the observed the deflationary signal. It is not clear where or what this storage zone might be. If the blockage occurs deeper below the SCR, then pressure changes during DI events would be expected to be the same in both reservoirs for both scenarios shown in Fig. 2B and D.

The two options for the ERZ connection (Fig. 2A and C) were discussed by Cervelli and Miklius (2003) in relation to DI events caused by a blockage between the reservoirs. They support a direct connection from the HMMR to the ERZ (Fig. 2A and B) because of the correlation between pressure changes in the HMMR and slightly later at Pu'u 'Ō'ō. In this scenario, the pressure head in the HMMR continues to drive magma outflux, causing rapid deflation of the HMMR as its volume decreases. The deflation is expected to follow an exponential-like decline as the falling pressure differential drives a proportionately lower flux rate (e.g. Lengliné et al., 2008). The removal of magma continues until the HMMR pressure head is too low to overcome the resistance to flow. At some point the blockage is breached or removed, and the influx of magma from the SCR resumes. As the HMMR is now at a lower pressure than the SCR there is a rapid re-inflation until the pressure levels reach an equilibrium (e.g. Haney et al., 2016). The extremely rapid re-inflation stage indicates that the conduit supplying magma to the HMMR is wide, supporting the high flux rate. The source of the magma during this phase maintains a high pressure-differential to drive the flux, suggesting that the reservoir is relatively large.

One key and relatively unexplored corollary for the model shown by Fig. 2A is the impact "upstream" of the blockage. The motivation for this work comes from the implications of this particular scenario. We test the model that DI events are caused by a blockage between the SCR and the HMMR under the conditions that magma supply is constant from depth to the SCR over DI time-scales and magma must flow from the SCR to the HMMR without leaving the system by any other means (i.e., magma does not flow directly to the ERZ, SWRZ or deep storage). We follow the assumption of Cervelli and Miklius (2003) and Anderson et al. (2015) that magma is lost from the HMMR to the ERZ or some part of the summit magma system, while acknowledging that this connection is not fully understood. We neglect magma compressibility and the relationship between magma and reservoir compressibility as it is low within the reservoirs (Anderson et al., 2015; Rivalta and Segall, 2008). If this blockage model is correct and the above conditions are met, then a volume of magma similar in magnitude to that lost from the HMMR during a DI event is expected to be added to the SCR. Thus we test the hypothesis that a volume increase in the SCR during the deflationary phase of a DI event produces detectable tilt deformation at the surface.

4. Data

DI events are best recorded by the summit tiltmeter network (Fig. 1), operated by the U.S. Geological Survey (USGS) Hawaiian Volcano

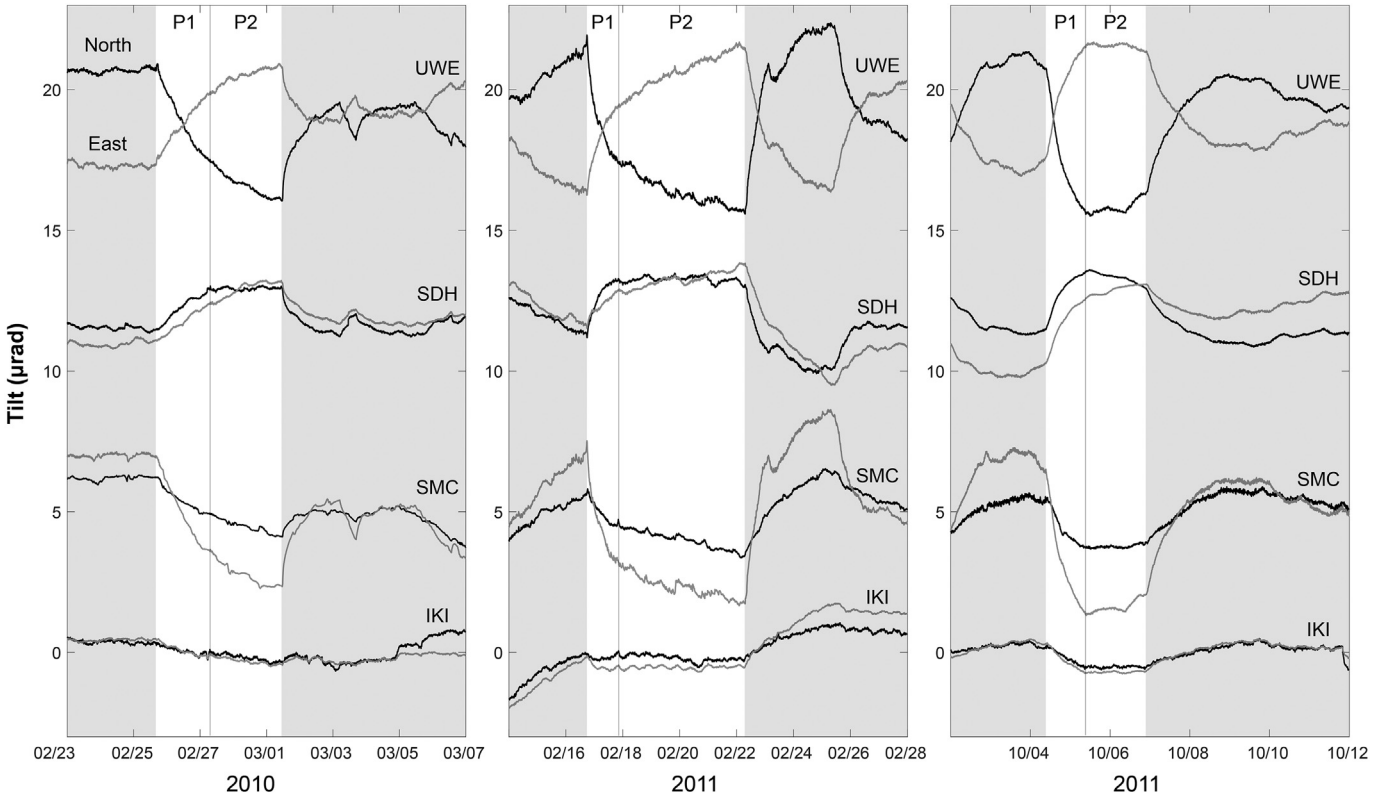

Fig. 3. North (black) and east (gray) tilt recorded on four tiltmeters (note variation in signals at each instrument). Examples of three DI events described in text showing differing characteristic patterns. Note the change in rate of deflation at various sites, indicated by vertical lines delineating Parts 1 (P1) and Parts 2 (P2) as defined in this study. P1 = onset of initial deflation through end of initial deflation rate, P2 = end of initial deflation rate to onset of rapid inflation.

Observatory (HVO) (Cervelli and Miklius, 2003; Anderson et al., 2015), but other, generally larger, events are also recorded in global positioning system (GPS), interferometric synthetic aperture radar (InSAR), and strain-meter data (Cervelli and Miklius, 2003; Dawson et al., 2004; Baker and Amelung, 2012; Poland et al., 2012). HVO tiltmeters record at a 1 min sampling rate and telemeter data back to the observatory. We use data from four summit tiltmeter sites surrounding the caldera that record DI events: UWE, SDH, SMC, and IKI. A fifth tiltmeter, ESC, is located along the ERZ but as it is ~5 km away from the summit it does not record DI events as clearly as the other sites, and is excluded from our analysis. The IKI site records events less clearly than the others. A rotational offset at the SMC tiltmeter has been suggested because tilt azimuths from this site are slightly discordant with those recorded at the other sites (Cervelli and Miklius, 2003; Anderson et al., 2015; Johnson et al., 2019). Although this tilt network is relatively small, it has a very favorable geometric distribution with respect to the active magma storage areas for resolving and distinguishing pressure changes in the different storage areas.

HVO maintains a catalogue of ~500 hand-picked DI events between the period January 1, 2000 to December 31, 2013 that identify the times of the onset of deflation, onset of inflation, and the end of rapid inflation. We analyzed the 16 largest (>4 μrad magnitude) DI events from the catalogue between 2010 and 2012 to test if tilt vectors at the summit sites suggested inflation from the SCR region. Outliers in the tilt data were cleaned using a median filter, and a diurnal signal estimation (Weron, 2010) was applied to reduce periodic noise for each of the selected time windows. The tilt data were then low-pass filtered and decimated down to a 5 min sample rate which is sufficient to resolve the temporal details of the DI events.

The selected events were categorized by HVO as U-type events based on their decreasing rate of deflation in an exponential-like or piecewise linear pattern over 1–3 days (Anderson et al., 2015), however the temporal evolution of the deflationary phase is variable among events (Fig. 3). Four events were characterized by well-defined exponentially decaying signals, and seven events consisted of two distinctly separate deflation phases, each exhibiting nearly linear tilt rates. The remaining events showed tilt beginning to increase slightly during the secondary phase before the onset of rapid inflation, which appears as a parabola-shaped time series.

For all events, the observed deflation signal was divided into two separate phases: an initial rapid deflationary phase (Part 1) followed by a secondary phase smaller in magnitude (Part 2) representing a lower rate of deflation. The onset of rapid inflation marks the end of the entire deflationary phase of the event. We chose to identify two separate phases of the deflationary period because the nature of the signals appears to be distinct and therefore may not be controlled by the same

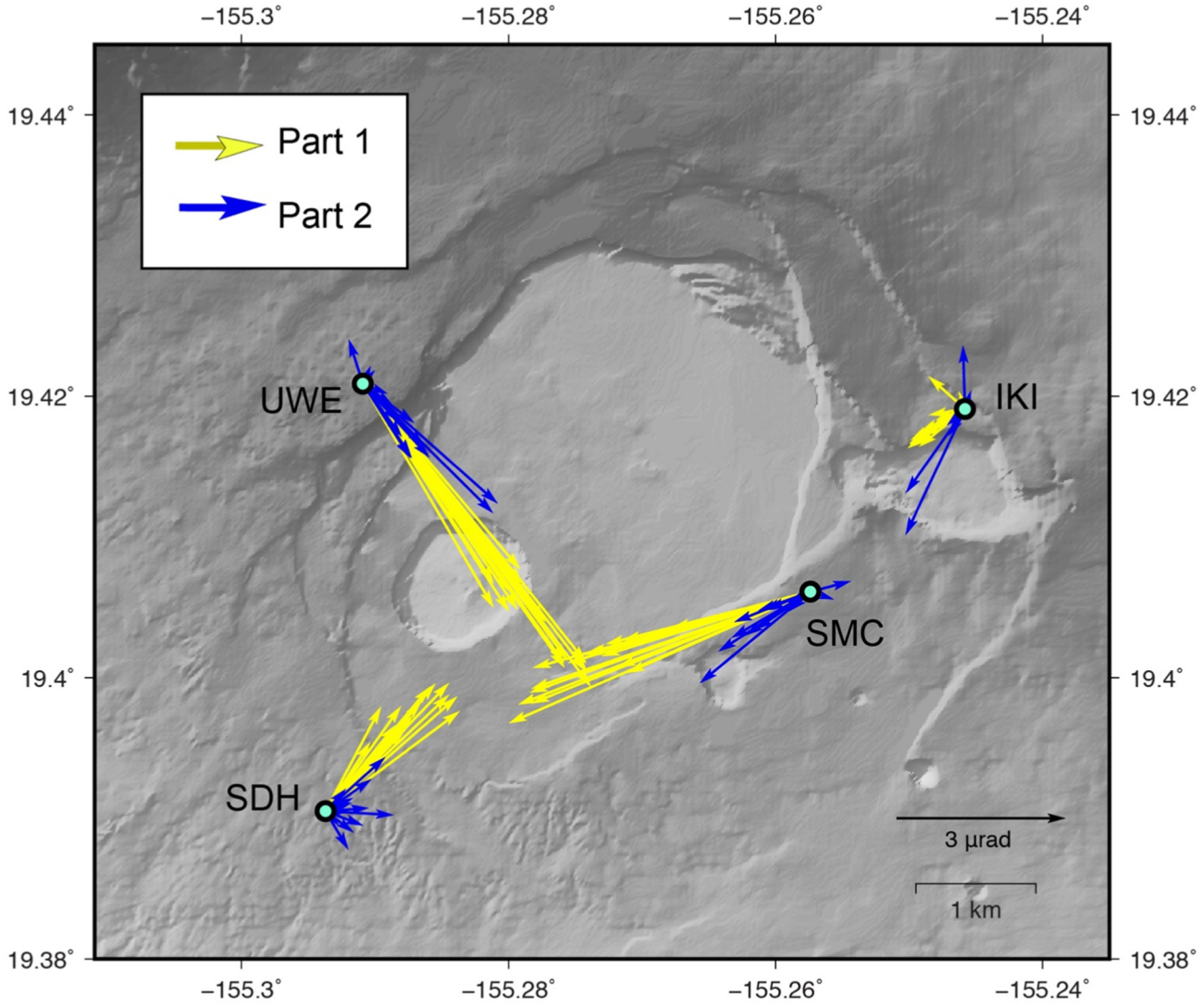

Fig. 4. Tilt observations for the 16 largest DI events between 2010 and 2012. Each event is divided into two parts: initial phase (Part 1) and secondary phase (Part 2). Note the decrease in magnitude, and difference in azimuthal direction of Part 2 compared to Part 1.

physical processes. Dividing these phases also allowed the tilt vectors for each phase to be viewed separately (Fig. 4) and provide a more detailed analysis than measuring a single magnitude of deflation over the entire event. The transition between Part 1 and Part 2 was hand-picked from the tilt data. Part 1 (initial deflation) is similar for all events, however, the temporal evolution of Part 2 (secondary phase) is variable.

Large magnitude DI events are also recorded by the network of GPS receivers on Kīlauea, although the signal to noise ratio in GPS data is much lower than for the tilt data. As it does not contribute significantly to our solutions, we do not include the GPS data in our modeling, but note that the distinction between DI parts 1 and 2 is observed at certain sites. For example, the transition to slower rates of deformation can be seen in a DI event recorded in GPS line-length changes across sites UWEV and CRIM in the north and east components (Fig. 5). GPS data in the vertical component were too noisy to detect a clear signal over these short time periods. The kinematic GPS solutions were produced from 30 s sample data files, cleaned, low-pass filtered, and decimated down to 30 min for the time windows of the DI event.

5. Predicted tilt from modeling geodetic sources

5.1. Magma reservoir deformation during DI events

We used deformation models to predict the tilt produced by a volume increase in a spherical (McTigue, 1987) and sill-like (Fialko et al., 2001) magma reservoir for a range of source depths and radii (Fig. 6). The goal was to determine if any combination of model parameters (source depth, radius, and volume change) for the SCR exists that would result in detectable DI tilt signals. The depth range was set to 500–5000 m depths and the radius range was 400–4000 m. The source center was set at the approximate horizontal location of the SCR determined by Poland et al. (2012).

Previous studies have estimated magma reservoir volume changes necessary to produce a given amount of tilt (Anderson et al., 2015; Dvorak and Dzurisin, 1993). The volume of blocked magma during DI events was estimated by Anderson et al. (2015) to be between 3.2×10^4 and 3.2×10^5 m^3, with 3.2×10^5 m^3 = 0.32 Mm^3. Dvorak and Dzurisin (1993), determined a conversion factor between annual scale tilt and volume change within the SCR to be 4.5×10^5 m^3 (0.00045 km^3) = 1 μrad of tilt at the UWE tiltmeter. Using the same approach, but adjusting the conversion factor to reflect that the dominant source for the DI events is the HMMR (which is closer to the UWE tiltmeter), we use a value of 0.35 Mm^3 in our analysis. This value produces tilts most similar in magnitude to the observations in this study.

For a spherical magma chamber, the pressure change and volume change can be related directly by $\Delta V = \pi \Delta p a^3/G$, where ΔV is the change in volume, Δp is change in pressure, a is radius, and G is the elastic shear modulus (Segall, 2013). Reorganizing the equation, the pressure change can be solved for given a radius and change in volume. The conversion between volume change and pressure change is more complex for a sill-like magma reservoir and was calculated using the opening of a penny-shaped crack (Fialko et al., 2001). During analysis volume changes are converted to pressure changes that are used as inputs to the deformation models.

The tilts were predicted at each of the four summit tiltmeters for a 0.35 Mm^3 volume increase in the SCR (Fig. 6). The results show that similar tilt magnitudes are produced using spherical and sill-like sources at each site. For a source at the previously estimated SCR depth range of 2.5–4 km and a range of radii, predicted tilts at SDH are between ~1 and 4 μrad to the west and <0.2 μrad to the north. Tilts predicted at site SMC were between ~1 and 4 μrad to the east and ~1 and 5 μrad to the north. Sites UWE and IKI produce smaller tilt magnitudes on the order of ~1 μrad. The deflation magnitudes of ~500 DI events cataloged by HVO are between 0.4 μrad and 8.5 μrad. The lower bound was set as a subjective estimate of the amplitude of non-magmatic signals in the data. This implies that DI related perturbations as small as 0.4 μrad can be detected, and that realistic changes in tilt magnitudes are not likely greater than ~8.5 μrad. Comparing these values with the results suggests that volume changes of the predicted magnitude range in the SCR alone would produce detectable deformation at all four tiltmeter sites, and particularly at sites SDH and SMC.

5.2. Deformation for volume increase in SCR and decrease in HMMR

The overall pattern of deformation during DI events implied by the scenario in Fig. 2A is produced by a volume decrease in the HMMR and simultaneous volume increase in the SCR. Both summit magma reservoirs were modeled to predict the deformation for a 0.35 Mm^3 volume decrease in the HMMR and simultaneous and equivalent volume increase in the SCR to test if SCR related deformation is detectable over HMMR deformation. The model configuration consists of two spherical sources (McTigue, 1987), with the HMMR at 700 m radius and 1000 m depth, and the SCR at 800 m radius and 3000 m depth. These parameters were selected based on plausible values (non-

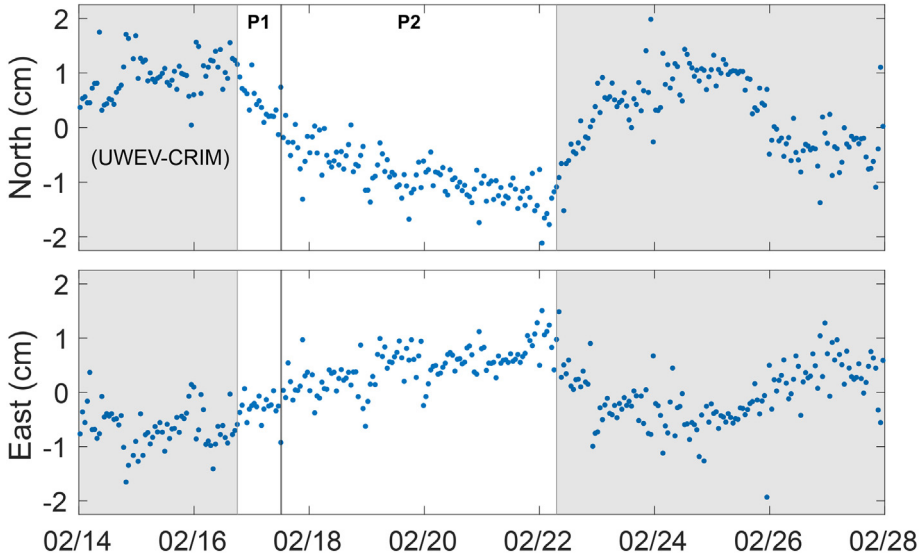

Fig. 5. DI event recorded in GPS line-length changes across summit sites UWEV - CRIM in February 2011. Vertical line separating Part 1(P1) and Part 2 (P2) was hand-picked from tilt data. Note change in rate of deformation between parts 1 and 2 in the north displacements.

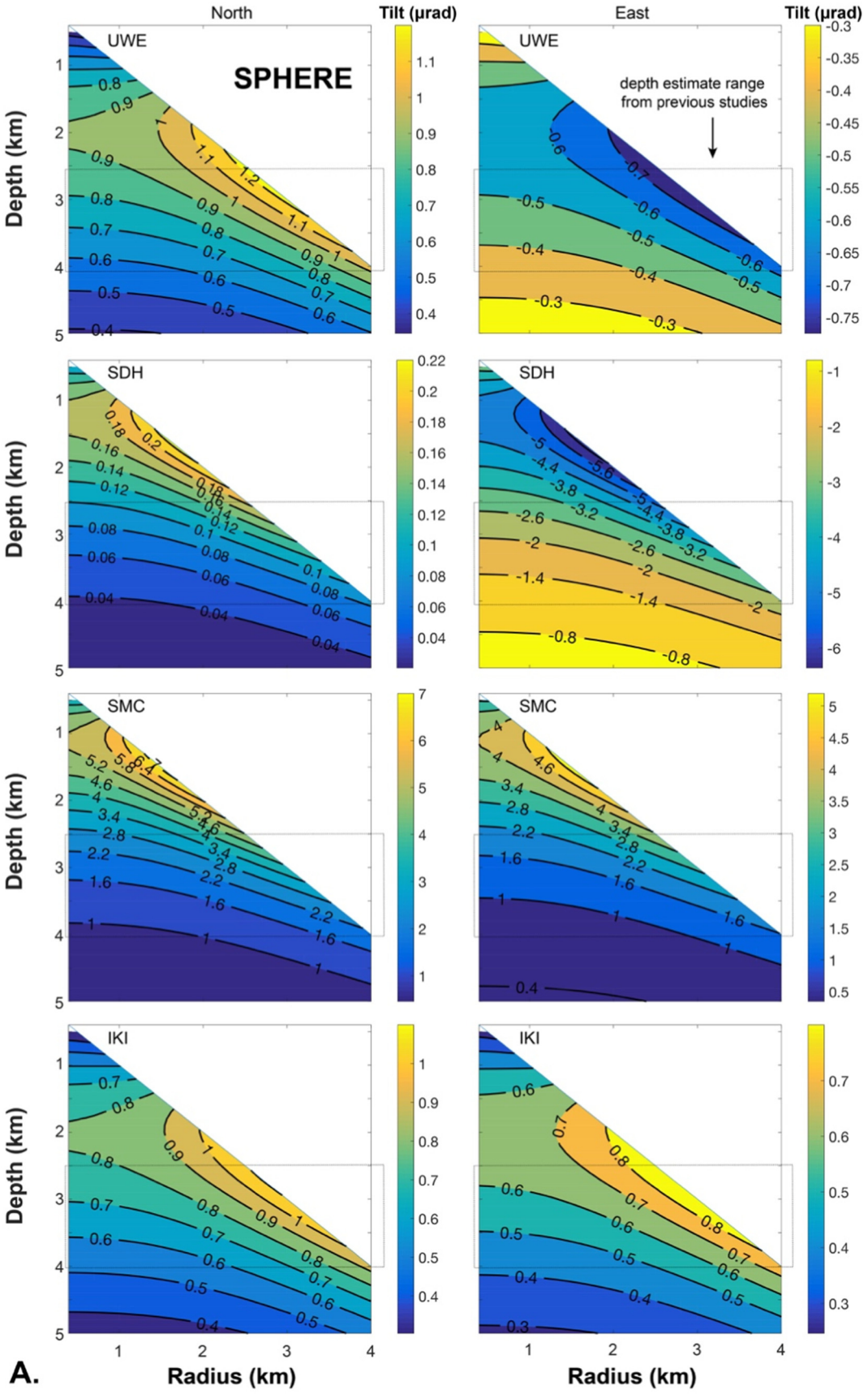

intersecting reservoirs and reservoir size not exceeding depth) from previous geodetic studies (Poland et al., 2012; Anderson et al., 2015; Baker and Amelung, 2012; Cervelli and Miklius, 2003).

We choose to model the SCR as a sphere, while acknowledging that it has been modeled by different geometries in other studies (e.g., Baker and Amelung, 2012; Poland et al., 2014). Fig. 6 shows that predicted tilt

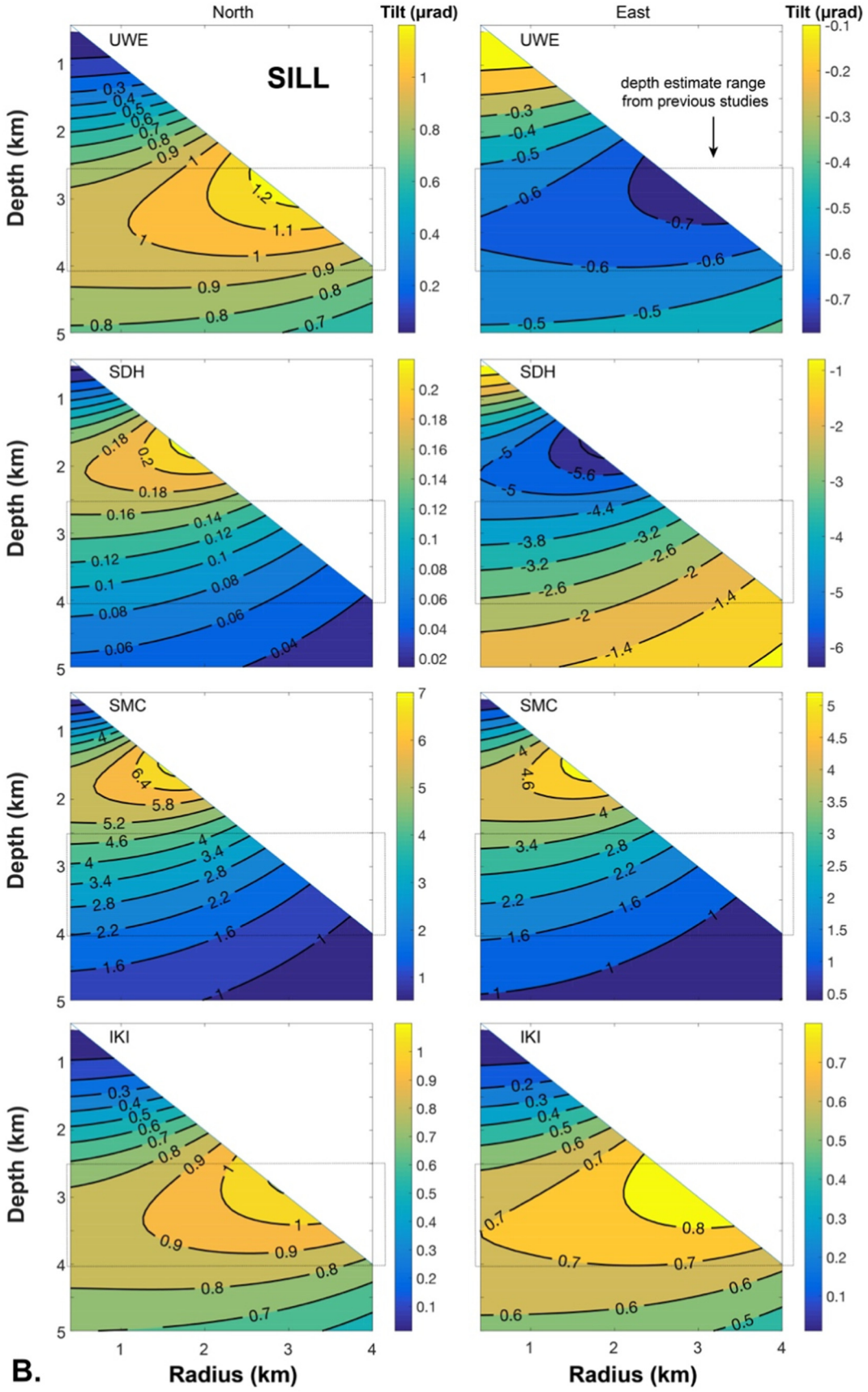

Fig. 6. Predicted north and east components of tilt (black contour lines) at the locations of the four summit tiltmeters for a 0.35 Mm^3 volume increase in A.) spherical and B.) sill-like (penny-shaped crack) geodetic sources located at the SCR horizontal location with depths 0.5–5 km and radii 0.4–4 km. All tilt values given in μrad. Tilt increases from dark blue to bright yellow. Only physically plausible reservoir depth and radius combinations are shown (source radius cannot be greater than depth). Box outlines approximate depth range estimates of SCR from previous studies.

magnitudes are similar for both spherical and sill-like sources, and therefore the choice of geodetic model shape does not significantly affect the analysis and interpretation. Each source deformation was predicted separately while requiring that the equivalent volume of magma removed from the HMMR is added to the SCR. The overall predicted deformation pattern was obtained by adding the deformation produced by both sources (Lisowski, 2007). We recognize that computing the deformation using two analytical models in close proximity neglects the interaction between the sources and violates the assumption of homogeneity. However, work investigating the effects of interacting source bodies by comparing results from analytical and numerical solutions (Pascal et al., 2014) indicates that for our geometry the errors introduced would be <16%.

The effect of the SCR pressure increase on the overall deformation is evident in the mapped predictions, with SCR related tilt causing a rotation of the tilt vectors (Fig. 7). The combined pattern of deformation shows ~30° of rotation at SDH and SMC away from the SCR source location, such that the predicted vectors no longer point to a single source at the HMMR as is observed for DI events (Cervelli and Miklius, 2003; Anderson et al., 2015). The influence of the SCR on the overall deformation pattern is most extreme in the east-west component of the SDH tiltmeter, which is located almost directly west of the approximate SCR location. Here, the predicted tilt from the HMMR is 2.8 μrad to the east, and the predicted tilt from the SCR is 2.0 μrad to the west, resulting in an overall tilt of 0.9 μrad to the east. At UWE the predicted HMMR tilt is 4.5 μrad to the south and 4.6 μrad to the east, while the SCR contribution is 0.7 μrad to the north and 0.5 μrad to the west. Combining these gives an overall tilt of 3.8 μrad to the south and 4.2 μrad to the east. The SCR contribution is not only greater than the average noise of tilt meters (0.1 μrad), but it is also above the threshold of the smallest DI event magnitude (0.4 μrad), and therefore should be a detectable contribution to the overall tilt signal, although the HMMR signal is greater in magnitude.

6. Analysis of selected DI events

When viewed spatially, tilt vectors for Part 1 point to a region east to southeast of Halemaʻumaʻu crater within the caldera (Fig. 4), consistent with previous studies. For Part 2, the magnitude of tilt vectors decreases, and azimuths tend to rotate away from the orientation of the initial deflation phase. At UWE, four of the Part 2 vector azimuths are consistent with the Part 1 azimuths, but the remaining vectors rotate slightly in the counterclockwise direction, which is what is predicted for an inflating SCR. Interestingly, the Part 2 vectors at SDH and SMC tend to rotate to

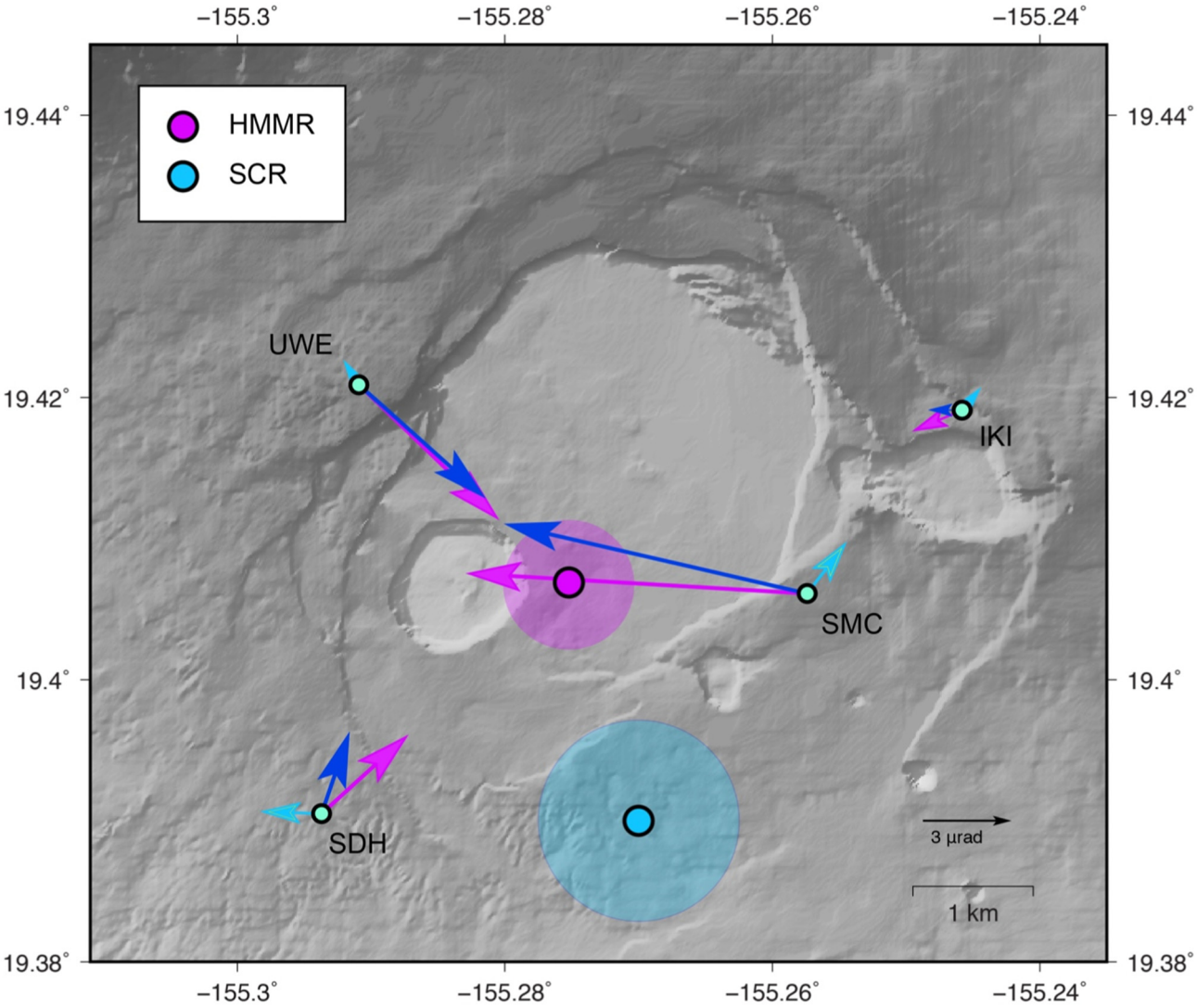

Fig. 7. Model predictions of tilt at Kīlauea summit for spherical sources representing the HMMR decreasing in volume by 0.35 Mm^3 (pink vectors), SCR increasing in volume by the same amount (light blue vectors), and total resulting tilt produced by adding both deformation signals (dark blue vectors). Shading around source locations indicates approximate modeled reservoir size.

the south, pointing towards the SCR, which is a rotation in the opposite direction of the predicted tilts for an inflating SCR. The range of Part 2 vector azimuths is most extreme at SDH, where vectors rotate clockwise up to ~120° from their initial positions. At IKI, although the DI events are less clear, a difference between Part 1 and 2 azimuths can still be observed.

6.1. Modeling

We searched for the volume change in the reservoirs that minimized the misfit between the model solutions and the observations in a least-squares sense. We used the non-linear optimization algorithm that employs the Nelder-Mead method (Matlab© fminsearch function) to find the best-fit parameters. The model configuration consisted of two spherical sources as described in Section 5.2, with constant source depth, radius, and horizontal location. Only the pressure change in each source was allowed to vary. Three models were tested: Model 1) The HMMR allowed to freely increase or decrease in pressure change with zero contribution from the SCR, Model 2) The HMMR allowed to freely decrease in pressure change, and the SCR defined as increasing in an "equivalent" pressure change (obtained using equivalent volume changes in each reservoir), and Model 3) Both the HMMR and the SCR allowed to independently increase or decrease in pressure change. The inputs were the observed steps in magnitude from the beginning and end of Part 1 and Part 2 for the north-south and east-west components at all sites, and the associated uncertainties. The model outputs the best-fitting pressure changes, which are then used to calculate the predicted deformation.

6.2. Model comparison

Tilts were predicted for each of the modeled pressure change solutions and compared with observed data to find the residuals between them. The AICc (Akaike Information Criterion with correction for small sample sizes) was calculated to identify the minimum AICc, indicating the preferred model. The AICc test absorbs the statistical impact of additional free parameters in describing the observations, allowing for an unbiased comparison of models with different degrees of freedom (A detailed description of the AICc calculations is given in Appendix A.)

Because we are primarily concerned with how our candidate models compare with each other, we construct the ΔAICc by subtracting the minimum AICc from all values. For each time period, the lowest ΔAICc is Model 3. Model 1 gives the second lowest AICc for each period, which is consistent with previous studies proposing that DI events manifest in the HMMR without observed contribution from the SCR (Cervelli and Miklius, 2003; Anderson et al., 2015). Model 2, which forces the SCR to increase by the same volume change as the HMMR decrease, consistently gives the highest ΔAICc of any model, indicating this model should be rejected as an explanation for the observed signals. These results support Model 3, a two-reservoir model with unconstrained pressure changes in the SCR, as the most representative model for the data. This implies that the SCR volume changes we find are not modeling random noise, but are describing a coherent signal.

6.3. Magma reservoir correlation

We calculated the Pearson's r correlation coefficients for the two data sets of predicted pressure changes in the HMMR and SCR (correlation coefficient calculations and values are given in Appendix B). This provides a measure of the strength of a linear relationship between the reservoirs and thus provides insight into how they are connected. A value of $r = 0$ implies that there is no linear correlation, and a value of $r = 1$ or -1 implies a positive or negative linear correlation, respectively. The calculated r coefficients were compared against the critical values of Pearson's r coefficient table for a two-tailed test, accounting for the degrees of freedom. For the relationship to be statistically significant, the calculated r value must exceed the critical r value.

For Parts 1 and 2, the reservoirs did not exhibit a statistically significant correlation at the 0.05 level. The lack of correlation between the HMMR and SCR for the matching time periods (HMMR Part 1 vs SCR Part 1, and HMMR Part 2 vs SCR Part 2) suggests that the relationship between the reservoirs is more complex than the simple conduit connection implied by Cervelli and Miklius (2003). A positive, nonzero correlation would be expected given an open conduit, and a negative one given a blockage between them. Because we are only looking at the total tilt offsets, the correlation refers to the total pressure changes only, and does not apply to the step by step temporal evolution of the DI event. There may be a range of time-varying pressure signals, but the general relationship between the reservoirs should be the same unless flux to the SCR stops immediately when the pressure increases. The HMMR during Part 1 and SCR during Part 2 were also not significantly correlated at the 0.05 level. This rules out the case where the reservoirs have different characteristic response times to changes in flux (Lengliné et al., 2008). This situation could have been an explanation for the lack of visible signal during Part 1 at the SCR as, if the SCR is much larger than the HMMR, it would respond more slowly to a net flux change. But in this case we would expect to see the signal from the SCR accumulating through the entire period, especially during Part 2, when there is little masking signal from the HMMR. The uncorrelated pressure signals during those time periods indicate that reservoir activities in the HMMR and SCR are unrelated to each other during DI events.

The only significant correlation found at the 0.05 level was between the SCR during Part 1 and the HMMR during Part 2 (Fig. 8). This negative correlation implies that for a given SCR pressure increase during Part 1, the HMMR pressure would decrease during Part 2, and vice versa. The correlation trend-line for SCR vs HMMR volume changes has a slope of approximately −2. The average change in volume in the SCR during Part 1 (0.155 Mm^3) and in the HMMR during Part 2 (0.013 Mm^3) has a ratio of 12:1, much larger than would be expected for the observed correlation trend of ~2. The range in predicted relative volume changes for each event makes it difficult to hypothesize a single representative process that characterizes all events. In addition, the correlation is not significant at the 0.01 level, and therefore, it remains plausible that this correlation at the 0.05 level may be a result of statistical analysis and does not represent a physically realistic scenario.

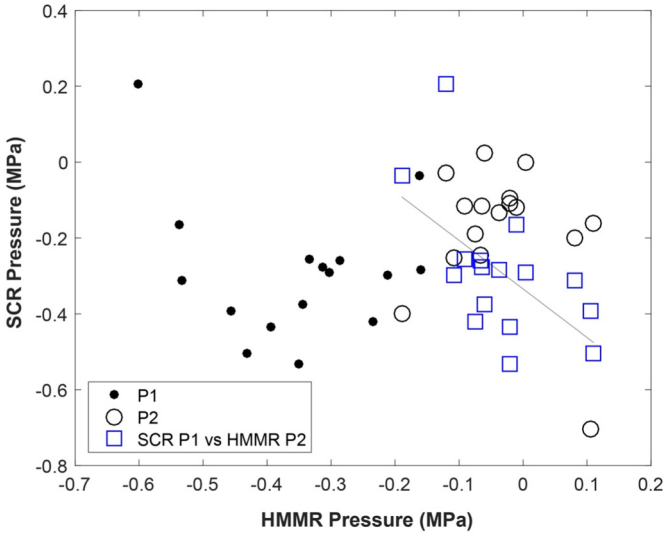

Fig. 8. Predicted pressure changes in the HMMR versus SCR for Model 3 during Part 1 (P1), Part 2 (P2) and for SCR P1 versus HMMR P2. Pearson's correlation coefficients are: P1, $r = -0.2029$; P2, $r = -0.2075$; and SCR P1 vs HMMR P2, $r = -0.5787$. Gray trend-line shown indicates the best fit least-squares linear correlation between SCR P1 vs HMMR P2 (slope = −1.3).

7. Discussion

Analysis of deformation implied by the configuration of Fig. 2A during DI events provides insight to Kīlauea's shallow magmatic system configuration as well as the processes driving magma reservoir activity. Our results favor a model with unconstrained pressure changes in both the HMMR and SCR, although Part 1 of the events are much more strongly associated with the HMMR than with the SCR. The AICc values also show that all models we tested describe Part 1 of the DI events better than Part 2. The better fit of the models may be because the tilts during Part 1 are larger in magnitude, have higher signal to noise ratio, and are more similar in orientation for all events than the variation exhibited during Part 2. This decrease in magnitude and inconsistency in azimuthal rotation suggests changes within the system that are not sufficiently described by the SCR alone.

The more complex deformation pattern during Part 2 may be a result of activity within other storage zones. Migrations of deformation centers at Kīlauea's summit have previously been documented, and it is suggested that they result from the interconnection of magma storage and transport areas that activate in response to accumulation or withdrawal of magma over time (Fiske and Kinoshita, 1969; Dieterich and Decker, 1975; Shimozuru, 1981; Ryan et al., 1981; Yang et al., 1992; Lockwood et al., 1999). It is possible the signals we observe in Part 2 are associated with small-scale pressure variations within some combination of these other zones.

The apparent relocation of the main source of deflation from east of Halemaʻumaʻu crater to south of the caldera observed between Parts 1 and 2 of some of the DI events, could reflect a migration of magma to another part of the system. Wright and Klein (2014) note that for many volcanic events at Kīlauea, such as those causing the varying Fiske and Kinoshita (1969) inflation centers from 1966 to 1967, deflation vectors may rotate clockwise from UWE. They interpret this rotation as initial draining of the northern region of the magmatic system, followed by draining of areas in the south. Although this may partially explain tilt rotations it does not explain the reduction in tilt rate at the onset of Part 2. At SDH and SMC, the tilt vector rotations towards the SCR location to the south could reflect a similar draining of the eastern Halemaʻumaʻu magmatic region during Part 1, followed by subsequent draining in the south during Part 2. The slight counterclockwise rotations generally observed at UWE during Part 2, however, are not consistent with draining of the SCR, and instead would imply inflation of a nearby source to the south. If these rotations at UWE were caused by the HMMR inflating slightly, it could be expected that the inflation would be detected at the other tiltmeter sites (Mogi, 1958; Lisowski, 2007), but this is not clearly observed as evidenced by the majority (13 of 16) of predicted pressures for Model 3 indicating deflation. The UWE tiltmeter could be detecting localized signals such as smaller magmatic storage zones, hydrological or hydrothermal system changes, stresses from faulting, or responses to changing rheological properties around the caldera rim. Because the Part 1 and 2 signals at UWE are larger than the 0.4 μrad DI event threshold, the observed rotations are outside the expected noise range and are therefore likely real signals. Similarly, while the tilt signals at site SDH could be influenced by local effects in the south caldera region (Dvorak and Okamura, 1987; Lockwood et al., 1999), we would expect the magnitude of these effects to be considerably smaller than the signals observed.

The overall deformation pattern may also be influenced by a misfit that has been suggested for the SMC tiltmeter, which generally points south of the approximate HMMR location (Anderson et al., 2015; Johnson et al., 2019). In a study on the effects of topography on tilt data, Johnson et al. (2019) found that surface geometry at Kīlauea can cause tilt rotations of ~10°, which could also be contributing to the observed signals. This topographic effect, however, only partially explains the anomalous tilt observed at site SMC. The UWE tiltmeter signals may also be influenced by topography, but their results suggested that tilt rotations were not impacted (Johnson et al., 2019).

Dvorak and Okamura (1987) suggested that the apparent exponential decay rate of summit tilt signals is controlled by magma flow rates and other similar properties, and that volcano rheology and migration of subsidence centers are not controlling factors. Anderson et al. (2015) suggested that some DI events could be caused by blockages deeper in the system. We agree that this interpretation is plausible. If the blockage occurs deeper than the SCR, the HMMR would rapidly deflate when magma exits to the ERZ, assuming it is not supplied by the SCR at a faster rate. During rapid HMMR deflation, magma would still be moving from the SCR to the HMMR because of the pressure difference between them, but the HMMR would not necessarily inflate since magma is being output to the ERZ at a higher rate than the recharge. Baker and Amelung (2012) proposed a similar top down model configuration. This model fits tilt observations for the most part, except for the counterclockwise rotation at the UWE site.

It is possible that SCR inflation during Part 1 may still be undetected, but this seems unlikely as the same amount of magma blocked would theoretically produce a large enough signal to be detected. If the best fitting model for Part 1 only includes HMMR deflation, the question remains of where the magma blocked from the HMMR is stored if a blockage occurs between the SCR and HMMR. Tilt observations over the course of the DI events reflect a more complex deformation pattern than the transfer of volume through a conduit connecting reservoirs implied by Fig. 2A. With the constraint of only four tiltmeters, a two-source geodetic model may not be able to accurately predict the complex deformation pattern. Further analysis could provide additional insight into how these events manifest.

The results suggesting a possible correlation between reservoirs over the two parts imply that for lower pressure changes in the SCR during Part 1, pressure changes are higher in the HMMR during Part 2. This may imply blockages in the system that have partially breached before completely opening, such that a fraction of the magma is transported into the HMMR during Part 2 before the blockage is fully breached during the rapid inflation. Partial blockages may also help to explain the variation in magnitude and degree of orientation of the tilt vectors for each event.

For our modeling we chose to fix the depth and radius for the HMMR based on values from previous studies (e.g., Cervelli and Miklius, 2003; Anderson et al., 2015), but a range of other reservoir geometries are plausible. Changing the geometry of our models, however, would not have a significant impact on the results of our analysis. If the HMMR was modeled deeper (Anderson et al., 2019), then the HMMR pressure change would need to be bigger to produce the same observed signal. Since we are using a mass balance approach, the SCR signal would then be larger due to the larger pressure change in the HMMR. This means even more SCR related tilt rotation would be expected, and the SCR would contribute more to the overall combined deformation. However, this SCR contribution is not observed. Changing the HMMR radius would have similar effects. For a given pressure change and depth, a larger source radius will result in larger signals, while a smaller radius will result in smaller signals. Anderson et al. (2019) estimated the HMMR volume to be between 2.3 and 5.4 km^3, which equates to a radius between ~840 and ~1090 m for a spherical reservoir. Fig. 6A shows the predicted deformation for a pressure change in a spherical reservoir at varying depths and radii, illustrating how the deformation is influenced by changing these parameters.

Finally, we note that although the dramatic events of the 2018 Kīlauea summit collapse sequence (Neal et al., 2019) have dramatically transformed the topography of the summit, the results presented here remain of current interest as recent deformation measurements indicate that the plumbing and storage system is being reoccupied, and that DI events have resumed (pers. comm. Ingrid Johanson, February 14, 2020).

8. Conclusions

Our results are inconsistent with the reservoir configuration proposed by Cervelli and Miklius (2003) and shown in Fig. 2A, suggesting a direct connection from the HMMR to the eruption site at Pu'u 'Ō'ō, and a direct connection between the SCR and HMMR which is temporarily blocked during DI events. Inflation of the SCR that would be expected during the HMMR deflation was not detected in our analysis. A blockage occurring below the SCR would imply deflation in both the HMMR and SCR during a DI event, but our results do not show a correlation between deflation in the reservoirs over the time periods analyzed.

Our results are also inconsistent with the configuration proposed by Poland et al. (2012), which consists of a direct connection between the SCR and HMMR, and the connection to Pu'u 'Ō'ō coming from the SCR. This configuration implies that a blockage between the SCR and HMMR should generate little signal from the HMMR, unless there is a "sink" for its magma somewhere locally, for which we are unware of supporting evidence. As with the Cervelli and Miklius (2003) configuration, if the blockage is below the SCR both reservoirs should experience similar pressure drops, which is not supported by our analysis.

Although our results do not provide a preferred candidate for the reservoir configuration and DI process, they do suggest that the HMMR and SCR do not have a simple connection between them, and that the summit reservoirs are instead perhaps more like the earlier conceptual models of the system consisting of a number reservoirs with their own source conduits connecting in some complex way to the deep magma source.

Acknowledgements

We thank Asta Miklius for her generous guidance and time assisting with understanding Kīlauea deformation, and the staff and scientists of the USGS Hawaiian Volcano Observatory for installing and maintaining the deformation network, and kindly providing the data on which studies such as this are based. We thank Michael Poland and Asta Miklius for their work picking DI events and maintaining the DI catalogue. We thank Kyle Anderson and Ingrid Johanson for their thorough reviews and comments which helped to significantly improve the manuscript. The tilt data used in this study are available from the USGS Hawaiian Volcano Observatory upon request. GPS rinex files are available from the UNAVCO archive. This work was supported in part by NSF grant # 1331125 (EAR - GEOPHYSICS).

Appendix A. Calculating ΔAICc

To calculate the ΔAICc values given in Table 1, the RSS (residual sum of squares) was first calculated using,

$$RSS = \sum_{i=1}^{n} \frac{\left(y_i - f_i\left(\hat{\theta}\right)\right)^2}{\sigma_i^2} \tag{A1}$$

where y is observed data, $f(\theta)$ is model predictions for which θ is the set of best fit parameters, σ is the uncertainty (error), the subscript i indicates the sample index, and n is the number of observations. The RSS was scaled by the squared error. In this case, $n = 4$ tilt sites $\times$ 2 components for each instrument (north and east) $\times$ 16 events $= 128$ observations. The AIC and AICc were calculated using the formulations,

$$AIC = 2k + n\ \ln(RSS) \tag{A2}$$

$$AICc = AIC + \frac{2k^2 + 2k}{n-k-1} \tag{A3}$$

where k is the number of parameters in the model. For Model 1 and Model 2, $k = 1$, and for Model 3, $k = 2$. These steps were done for Part 1 (AIC_1) and Part 2 (AIC_2) separately, and combined to give the entire event ($AIC_{\text{Entire event}}$). These were given by,

$$AIC_1 = 2k + n\ \ln(RSS_{P1})$$

$$AIC_2 = 2k + n\ \ln(RSS_{P2})$$

$$AIC_{Entire\ event} = 2k + n\ \ln(RSS_{P1} + RSS_{P2})$$

where RSS_{P1} and RSS_{P2} are the RSS for Part 1 and Part 2, respectively. The AICc was then calculated using Eq. (A3). Finally, the ΔAICc was calculated by subtracting the minimum AICc value of all the results.

$$\Delta AICc = AICc - AICc_{min} \tag{A4}$$

The ΔAICc was calculated for each model, and the values then compared. The lowest value indicates the preferred model.

Table 1
ΔAICc results for three models tested: Model 1) The HMMR allowed to freely increase or decrease in pressure change; Model 2) The HMMR allowed to freely decrease in pressure change, and the SCR set to increase in an "equivalent" pressure change (for equivalent volume changes in each reservoir), and Model 3) Both the HMMR and the SCR allowed to freely increase or decrease in pressure change.

Period	Model 1	Model 2	Model 3
Part 1	94.8	197.5	0.00
Part 2	180.3	205.3	117.5
Entire event	233.3	290.2	160.5

Appendix B. Calculating correlation coefficients

The correlation coefficients were calculated using Pearson's product moment correlation coefficient r, which measures the linear correlation between two variables x and y. The formulation is given by,

$$r = \frac{\sum_{i=1}^{n}(x_i - \overline{x})(y_i - \overline{y})}{\sqrt{\sum_{i=1}^{n}(x_i - \overline{x})^2}\sqrt{\sum_{i=1}^{n}(y_i - \overline{y})^2}}$$

where x_i and y_i are the sample points indexed with i, $\overline{x}$ and $\overline{y}$ are the sample means, and n is the sample size. A value of $r = 0$ implies that there is no linear correlation between the variables, and a value of 1 or -1 implies that data points lie on a line of x and y. We calculated the correlation coefficients for the predicted reservoir pressure changes for 16 DI events in the following pairs:

- r_{P1} → HMMR Part 1 and SCR Part 1
- r_{P2} → HMMR Part 2 and SCR Part 2
- r_{P1+P2} → HMMR Part 1 + Part 2 and SCR Part 1 + Part 2
- r_{HMMRP1_SCRP2} → HMMR Part 1 and SCR Part 2
- r_{SCRP1_HMMRP2} → SCR Part 1 and HMMR Part 2

The calculated Pearson's r correlation coefficients were compared against the critical values in the Pearson's r coefficient table, taking into account the degrees of freedom (df), where df = the number of pairs of scores minus 2. In our case, there were 14 degrees of freedom (16 events – 2). To be considered a significantly nonzero correlation at the 0.05 and 0.01 levels, the calculated r statistic must exceed the critical table value $r_{critical}$ for 14 degrees of freedom. The results are shown below:

At the **0.01** level of significance, $r_{critical} = 0.623$.
$r_{P1} = 0.2029 < r_{critical} = 0.623$
$r_{P2} = 0.2075 < r_{critical} = 0.623$
$r_{P1+P2} = 0.6011 < r_{critical} = 0.623$
$r_{HMMRP1\_SCRP2} = |-0.0861| < r_{critical} = 0.623$
$r_{SCRP1\_HMMRP2} = |-0.5787| < r_{critical} = 0.623$

At the **0.05** level of significance, $r_{critical} = 0.497$.

$r_{P1} = 0.2029 < r_{critical} = 0.497$

$r_{P2} = 0.2075 < r_{critical} = 0.497$

$r_{P1+P2} = 0.6011 > r_{critical} = 0.497$

$r_{HMMRP1\_SCRP2} = |-0.0861| < r_{critical} = 0.497$

$r_{SCRP1\_HMMRP2} = |-0.5787| > r_{critical} = 0.497$

At the 0.01 level, all results are non-significant (accept null hypothesis). At the 0.05 level, results are non-significant during Part 1 and Part 2 separately, but the result is significant for Part 1 + Part 2 (reject null hypothesis). This suggests that the HMMR and SCR are not correlated for Part 1 and Part 2 individually, but that over the course of the DI event there is a negative correlation between them. To find the source of the correlation over the entire event, we tested for correlation between reservoirs over both parts. For Part 1 in the HMMR and Part 2 in the SCR, $r = -0.0861$ (non-significant result). For Part 1 in the SCR and Part 2 in the HMMR, $r = -0.5787$ (significant result at the 0.05 level). This revealed that there was a statistically significant correlation at the 0.05 level for the pressure changes in the SCR during Part 1 and the HMMR during Part 2.

References

Almendros, J., Chouet, B., Dawson, P., Bond, T., 2002. Identifying elements of the plumbing system beneath Kilauea Volcano, Hawaii, from the source locations of very-long-period signals. Geophys. J. Int. 148, 303–312.

Anderson, K, Lisowski, M, Segall, P, 2010. Cyclic ground tilt associated with the 2004-2008 eruption of Mount St. Helens. Journal of Geophysical Research 115 (B11), 29. https://doi.org/10.1029/2009JB007102.

Anderson, K.R., Poland, M.P., Johnson, J.H., Miklius, A., 2015. Episodic deflation-inflation events at Kīlauea Volcano and implications for the shallow magma system. In: Carey, R., Poland, M., Cayol, V., Weis, D. (Eds.), Hawaiian Volcanism: From Source to Surface. American Geophysical Union Geophysical Monograph Series 208, pp. 229–250.

Anderson, K., Johanson, I., Patrick, M., Gu, M., Segall, P., Poland, M., Montgomery-Brown, E., Miklius, A., 2019. Magma reservoir failure and the onset of caldera collapse at Kīlauea Volcano in 2018. Science 366, eaaz1822. https://doi.org/10.1126/science.aaz1822.

Baker, S., Amelung, F., 2012. Top-down inflation and deflation at the summit of Kīlauea Volcano, Hawai'i observed with InSAR. Journal of Geophysical Research: Solid Earth 117 (B12406) (14 pp.).

Battaglia, J., Got, J.-L., Okubo, P., 2003. Location of long-period events below Kilauea Volcano using seismic amplitudes and accurate relative relocation. J. Geophys. Res. 108 (B12) (p. ESE 2-1 to ESE 2-16).

Cervelli, P.F., Miklius, A., 2003. The shallow magmatic system of Kilauea Volcano. In: Heliker, C.C., Swanson, D.A., Takahashi, T.J. (Eds.), U.S. Geological Survey Professional Paper 1676. The Pu'u "O"o-Kupaianaha Eruption of Kilauea Volcano, Hawai'i: The First 20 Years, pp. 149–163.

Chouet, B.A., Dawson, P.B., James, M.R., Lane, S.J., 2010. Seismic source mechanism of degassing bursts at Kilauea Volcano, Hawaii: results from waveform inversion in the 10-50 s band. J. Geophys. Res. 115 (B09311) (24 pp.).

Dawson, P.B., Chouet, B.A., Okubo, P.G., Villasenor, A., Benz, H.M., 1999. Three-dimensional velocity structure of the Kilauea caldera, Hawaii. Geophys. Res. Lett. 26 (18), 2805–2808.

Dawson, P., Whilldin, D., Chouet, B., 2004. Application of near real-time radial semblance to locate the shallow magmatic conduit at Kilauea Volcano, Hawaii. Geophys. Res. Lett. 31 (21), 1–4. https://doi.org/10.1029/2004GL021163 L21606.

Delaney, P.T., Fiske, R.S., Miklius, A., Okamura, A.T., Sako, M.K., 1990. Deep magma body beneath the summit and rift zones of Kilauea Volcano, Hawaii. Science 247 (March 16), 1311–1316.

Delaney, P.T., Miklius, A., Arnadottir, T., Okamura, A.T., Sako, M.K., 1993. Motion of Kilauea Volcano during sustained eruption from the Puu Oo and Kupaianaha vents, 1983–1991. J. Geophys. Res. 98 (B10), 17,801–817,820.

Denlinger, R.P., 1997. A dynamic balance between magma supply and eruption rate at Kilauea Volcano, Hawaii. J. Geophys. Res. 102 (B8), 18,091–018,100.

Dieterich, J.H., Decker, R.W., 1975. Finite element modeling of surface deformation associated with volcanism. J. Geophys. Res. 80 (29), 4094–4102.

Dvorak, J.J., Dzurisin, D., 1993. Variations in magma supply rate at Kilauea Volcano, Hawaii. J. Geophys. Res. 98 (B12), 22,255–22,268.

Dvorak, J.J., Dzurisin, D., 1997. Volcano geodesy: the search for magma reservoirs and the formation of eruptive vents. Rev. Geophys. 35 (3), 343–384.

Dvorak, J.J., Okamura, A.T., 1987. A hydraulic model to explain variations in summit tilt rate at Kilauea and Mauna Loa Volcanoes. In: Decker, R.W., Wright, T.L., Stauffer, P.H. (Eds.), U.S. Geological Survey Professional Paper 1350. Volcanism in Hawaii, pp. 1281–1296.

Dzurisin, D., Anderson, L.A., Eaton, G.P., Koyanagi, R.Y., Lipman, P.W., Lockwood, J.P., Okamura, R.T., Puniwai, G.S., Sako, M.K., Yamashita, K.M., 1980. Geophysical observations of Kilauea Volcano, Hawaii, 2. Constraints on the magma supply during November 1975–September 1977. In: McBirney, A.R. (Ed.), Journal of Volcanology and Geothermal Research. Gordon A. Macdonald Memorial Volume (Special Issue), pp. 241–269.

Eaton, J, Murata, K, 1960. How Volcanoes grow: Science. Science 132, 925–938.

Fialko, Y., Khazan, Y., Simons, M., 2001. Deformation due to a pressurized horizontal circular crack in an elastic half-space, with applications to volcano geodesy. Geophys. J. Int. 146 (1), 181–190. https://doi.org/10.1046/j.1365-246X.2001. 00452.x.

Fiske, R.S., Kinoshita, W.T., 1969. Inflation of Kilauea Volcano prior to its 1967–1968 eruption. Science 165, 341–349.

Fiske, R.S., Swanson, D.A., Wright, T.L., 1993. A model of Kilauea Volcano's rift-zone magma system [abs.]. Eos, Transactions, American Geophysical Union 74 (43), 646 supp..

Genco, R., Ripepe, M., 2010. Inflation-deflation cycles revealed by tilt and seismic records at Stromboli volcano. Geophys. Res. Lett. 37 (12).

Haney, M.M., Patrick, M.R., Anderson, K.R., 2016. Ground Tilt Time Delays Between Kilauea Volcano's Summit and East Rift Zone Caused by Magma Reservoir Buffering [abs.]. Eos Transactions AGU, Fall Meeting Suppl. 2016: Abstract V12A-06H.

Heliker, C.C., Mattox, T.N., 2003. The first two decades of the Pu'u 'O'o-Kupaianaha eruption: chronology and selected bibliography. In: Heliker, C.C., Swanson, D.A., Takahashi, T.J. (Eds.), U.S. Geological Survey Professional Paper 1676. The Pu'u "O"o-Kupaianaha Eruption of Kilauea Volcano, Hawai'i: The First 20 Years, pp. 1–27.

Holcomb, R.T., 1987. Eruptive history and long-term behavior of Kilauea Volcano. In: Decker, R.W., Wright, T.L., Stauffer, P.H. (Eds.), U.S. Geological Survey Professional Paper 1350. Volcanism in Hawaii, pp. 261–350.

Johnson, D.J., 1992. Dynamics of magma storage in the summit reservoir of Kilauea Volcano, Hawaii. J. Geophys. Res. 97 (B2), 1807–1820.

Johnson, D.J., Eggers, A.A., Bagnardi, M., Battaglia, M., Poland, M.P., Miklius, A., 2010. Shallow magma accumulation at Kilauea Volcano, Hawai'i, revealed by microgravity surveys. Geology 38 (12), 1139–1142.

Johnson, J., Poland, M., Anderson, K., Biggs, J., 2019. A cautionary tale of topography and tilt from Kīlauea Caldera. Geophys. Res. Lett. 46 (8), 4221–4229. https://doi.org/10.1029/2018gl081757.

Klein, F.W., Koyanagi, R.Y., Nakata, J.S., Tanigawa, W.R., 1987. The seismicity of Kilauea's magma system. In: Decker, R.W., Wright, T.L., Stauffer, P.H. (Eds.), U.S. Geological Survey Professional Paper 1350. Volcanism in Hawaii, pp. 1019–1185.

Lengliné, O., Marsan, D., Got, J.-L., Pinel, V., Ferrazzini, V., Okubo, P.G., 2008. Seismicity and deformation induced by magma accumulation at three basaltic volcanoes. J. Geophys. Res. 113 (B12305).

Lisowski, M., 2007. Analytical volcano deformation source models. In: Dzurisin, D. (Ed.), Volcano Deformation: Geodetic Monitoring Techniques. Springer Verlag, Germany, in association with Praxis Publishing, Ltd., UK, Berlin, Germany, and Chichester, UK, pp. 279–304.

Lockwood, J.P., Tilling, R.I., Holcomb, R.T., Klein, F., Okamura, A.T., Peterson, D.W., 1999. Magma migration and resupply during the 1974 summit eruptions of Kilauea Volcano, Hawai'i. U.S. Geological Survey Professional Paper 1613 (37 pp.).

Lundgren, P., Poland, M., Miklius, A., Orr, T., Yun, S.-H., Fielding, E., Liu, Z., Tanaka, A., Szeliga, W., Hensley, S., Owen, S., 2013. Evolution of dike opening during the March 2011 Kamoamoa fissure eruption, Kīlauea Volcano, Hawai'i. Journal of Geophysical Research, Solid Earth 118 (B3), 897–914.

McTigue, D.F., 1987. Elastic stress and deformation near a finite spherical magma body: resolution of the point source paradox. J. Geophys. Res. 92 (B12), 12, 931–912, 940.

Mogi, K., 1958. Relations between the eruptions of various volcanoes and the deformations of the ground surfaces around them. Bulletin of the Earthquake Research Institute of the University of Tokyo 36, 111–123.

Montgomery-Brown, E.K., Sinnett, D.K., Poland, M., Segall, P., Orr, T., Zebker, H., Miklius, A., 2010. Geodetic evidence for en echelon dike emplacement and concurrent slow slip during the June 2007 intrusion and eruption at Kīlauea volcano, Hawaii. J. Geophys. Res. 115 (B07405) (15 pp.).

Myer, D., Sandwell, D., Brooks, B., Foster, J., Shimada, M., 2008. Inflation along Kilauea's Southwest Rift Zone in 2006. J. Volcanol. Geotherm. Res. 177 (2), 418–424.

Neal, C.A., et al., 2019. The 2018 rift eruption and summit collapse of Kīlauea Volcano. Science 363 (6425), 367–374. https://doi.org/10.1126/science.aav7046.

Ohminato, T., Chouet, B.A., Dawson, P.B., Kedar, S., 1998. Waveform inversion of very long period impulsive signals associated with magmatic injection beneath Kilauea Volcano, Hawaii. J. Geophys. Res. 103 (B10), 23,839–823,862.

Okubo, P.G., Nakata, J.S., Koyanagi, R.Y., 2014. The evolution of seismic monitoring systems at the Hawaiian Volcano Observatory. In: Poland, M.P., Takahashi, T.J., Landowski, C.M. (Eds.), U.S. Geological Survey Professional Paper 1801. Characteristics of Hawaiian Volcanoes, pp. 66–95.

Orr, T.R., Thelen, W.A., Patrick, M.R., Swanson, D.A., Wilson, D.C., 2013. Explosive eruptions triggered by rockfalls at Kīlauea volcano, Hawai'i. Geology 41 (2), 207–210.

Owen, S., Segall, P., Lisowski, M., Miklius, A., Murray, M., Bevis, M., Foster, J., 2000. January 30, 1997 eruptive event on Kilauea Volcano, Hawaii, as monitored by continuous GPS. Geophys. Res. Lett. 27 (17), 2757–2760.

Pascal, K., Neuberg, J., Rivalta, E., 2014. On precisely modelling surface deformation due to interacting magma chambers and dykes. Geophys. J. Int. 196, 253–278. https://doi.org/10.1093/gji/ggt343.

Patrick, M.R., Orr, T.R., 2013. Controls on lava lake level at Halema'uma'u Crater, Kilauea Volcano [abs.]. American Geophysical Union, Fall Meeting 2013 Abstracts: Abstract No. V52C-04.

Patrick, M.R., Orr, T.R., Sutton, A.J., Elias, T., Swanson, D.A., 2013. The first five years of Kīlauea's summit eruption in Halema'uma'u Crater, 2008–2013. U.S. Geological Survey Fact Sheet 2013-3116 (4 pp.).

Poland, M.P., Huth, T.E., Miklius, A., 2009a. Source processes of short-term, transient tilt events at Kilauea Volcano, Hawaii [abs.]. Eos, Transactions, American Geophysical Union 90 (52) supp.. (abstract no. V43G-2331).

Poland, M.P., Sutton, A.J., Gerlach, T.M., 2009b. Magma degassing triggered by static decompression at Kilauea Volcano, Hawai'i. Geophys. Res. Lett. 36 (L16306) (5 pp.).
Poland, M.P., Miklius, A., Sutton, A.J., Thornber, C.R., 2012. A mantle-driven surge in magma supply to Kīlauea Volcano during 2003–2007. Nat. Geosci. 5 (4), 295–300.
Poland, M.P., Miklius, A., Montgomery-Brown, E.K., 2014. Magma supply, storage, and transport at shield-stage Hawaiian volcanoes. In: Poland, M.P., Takahashi, T.J., Landowski, C.M. (Eds.), U.S. Geological Survey Professional Paper 1801. Characteristics of Hawaiian Volcanoes, pp. 178–235.
Rivalta, E., Segall, P., 2008. Magma compressibility and the missing source for some dike intrusions. Geophys. Res. Lett. 35 (4), L04306. https://doi.org/10.1029/2007GL032521.
Ryan, M.P., Koyanagi, R.Y., Fiske, R.S., 1981. Modeling the three dimensional structure of macroscopic magma transport systems: application to Kilauea Volcano, Hawaii. J. Geophys. Res. 86 (B8), 7111–7129.
Segall, P., 2013. Volcano deformation and eruption forecasting. Geol. Soc. Lond., Spec. Publ. 380 (1), 85–106.
Segall, P., Cervelli, P., Owen, S., Lisowski, M., Miklius, A., 2001. Constraints on dike propagation from continuous GPS measurements. J. Geophys. Res. 106 (B9), 19,301–319,317.
Shimozuru, D., 1981. Magma reservoir systems inferred from tilt patterns. Bull. Volcanol. 44 (3), 499–504.
Swanson, D.A., Duffield, W.A., Jackson, D.B., Peterson, D.W., 1979. Chronological narrative of the 1969-71 Mauna Ulu eruption of Kilauea Volcano, Hawaii. U.S. Geological Survey Professional Paper 1056 (55 pp.).
Tilling, R.I., 1987. Fluctuations in surface height of active lava lakes during 1972–1974 Mauna Ulu eruption, Kilauea Volcano, Hawaii. J. Geophys. Res. 92 (B13), 13,721–713,730.
Tilling, R, Dvorak, J, 1993. Anatomy of a basaltic volcano. Nature 363, 125–133.
Voight, B., Hoblitt, R.P., Clarke, A.B., Lockhart, A.B., Miller, A.D., Lynch, L., McMahon, J., 1998. Remarkable cyclic ground deformation monitored in real-time on Montserrat, and its use in eruption forecasting. Geophys. Res. Lett. 25 (18), 3405–3408.
Weron, R., 2010. REMST: MATLAB function to remove trend and seasonal component using the moving average method. Statistical Software Components M429001. Boston College Department of Economics.
Wolfe, E.W., Garcia, M.O., Jackson, D.B., Koyanagi, R.Y., Neal, C.A., Okamura, A.T., 1987. The Puu Oo eruption of Kilauea Volcano, episodes 1–20, January 3, 1983, to June 8, 1984. In: Decker, R.W., Wright, T.L., Stauffer, P.H. (Eds.), U.S. Geological Survey Professional Paper 1350. Volcanism in Hawaii, pp. 471–508.
Wright, T.L., Klein, F.W., 2014. Two hundred years of magma transport and storage at Kilauea Volcano, Hawai'i, 1790–2008. U.S. Geological Survey Professional Paper 1806 (240 pp.).
Yamashina, K.i., Matsushima, T., Ohmi, S., 1999. Volcanic deformation at Unzen, Japan, visualized by a time-differential stereoscopy. J. Volcanol. Geotherm. Res. 89 (1), 73–80.
Yang, X., Davis, P.M., Delaney, P.T., Okamura, A.T., 1992. Geodetic analysis of dike intrusion and motion of the magma reservoir beneath the summit of Kilauea Volcano, Hawaii: 1970–1985. J. Geophys. Res. 97 (B3), 3305–3324.